Induction of bronchus-associated lymphoid tissue by common zoonotic microorganisms, and establishment of a method for its quantification in whole lung lobes

David Twapokera Mzinza

Institute of Immunology, Hannover Medical School

University of Veterinary Medicine Hannover

2017

University of Veterinary Medicine Hannover

Institute of Immunology, Hannover Medical School

Induction of bronchus-associated lymphoid tissue by common zoonotic microorganisms, and establishment of a method for its quantification in whole lung lobes

THESIS

Submitted in partial fulfilment of the requirements for the degree

DOCTOR OF PHILOSOPHY

(PhD)

awarded by the University of Veterinary Medicine Hannover

by

David Twapokera Mzinza

Chitipa, Malawi

Hannover, Germany 2017

Supervisor: Prof. Dr. Reinhold Förster

Supervision group: Prof. Dr. Reinhold Förster

Prof. Dr. Peter Valentin-Weigand

Prof. Dr. Susanne Häußler

1st Evaluation: Prof. Dr. Reinhold Förster (Institute of Immunology, Hannover Medical School, Hannover, Germany)

Prof. Dr. Peter Valentin-Weigand (Institute for Microbiology, University of Veterinary Medicine Hannover, Hannover, Germany)

Prof. Dr. Susanne Häußler (Institute of Molecular Bacteriology, TWINCORE, Hannover, Germany and Department of Molecular Bacteriology Helmholtz Centre for Infection Research, Braunschweig, Germany)

2nd Evaluation: Prof. Jens Stein (Theodor Kocher Institute, University of Bern, Bern, Switzerland)

Date of final exam: 02/11/2017

I dedicate this work to Noella, Josiah, and Timothy.

This PhD project was supported by a Lichtenberg-Stipend through the University of Veterinary Medicine Hannover and additional funds from the Institute of Immunology, Hannover Medical School (German Excellence Initiative grant EXC62 – Rebirth; and SFB 900/B1).

Table of contents

Abbreviations

2D	two-dimension
3D	three-dimension
3DISCO	three-dimensional imaging of solvent-cleared organs
AF	autofluorescence
BALT	bronchus-associated lymphoid tissue
BHI	brain heart infusion
Cardif	caspase activation and recruitment domain adaptor inducing IFN-β
CCL	C-C chemokine ligand
CCR	C-C chemokine receptor
CD	cluster of differentiation
CFU	colony forming unit
CLARITY	clear lipid-exchanged Acrylamide-hybridized rigid imaging/immunostaining/in-situ-hybridization-compatible tissue hydrogel
CPS	capsular polysaccharide
CUBIC	clear, unobstructed brain/body imaging of solvent-cleared organs
CXCL	C-X-C chemokine ligand
CXCR	C-X-C chemokine receptor
DAPI	4’,6-dianidino-2-phenylindole
DBE	dibenzyl ether
DC	dendritic cell
DSLM	digitally scanned light sheet-based fluorescence microscopy
E. coli	*Escherichia coli*
EF	extracellular factor
EGFP	enhanced green fluorescent protein

FDC	follicular dendritic cell
HEV	high endothelial venule
Id2	inhibiter of differentiation 2
iDISCO	immunolabelling-enabled three-dimensional imaging of solvent-cleared organs
IFN	interferon
IFNαR	interferon alpha receptor
IgA	immunoglobulin A
IgD	immunoglobulin D
IgM	Immunoglobulin M
IL	interleukin
LPS	lipopolysaccharide
LTα	lymphotoxin alpha
LTβ	lymphotoxin beta
LTβR	lymphotoxin beta receptor
LiSM	light sheet microscopy
L. monocytogenes	*Listeria monocytogenes*
LT	lymphotoxin
LTi	lymphoid inducer cell
Lyve	lymphatic vessel endothelial hyaluronan receptor
MCP	monocyte chemoattractant protein
ml	millilitre
MRA	muraminidase released protein
MTB	*Mycobacterium tuberculosis*
MVA	modified vaccinia virus Ankara
MyD	myeloid differentiation

NALT	nasal-associated lymphoid tissue
^{o}C	degrees Celsius
OPFOS	orthogonal plane fluorescence and optical sectioning
OT-I	ovalbumin-specific CD8+ T cells
OVA	ovalbumin
PAMP	pathogen-associated molecular pattern
P. aeruginosa	*Pseudomonas aeruginosa*
PBS	phosphate-buffered saline
PCN	protein cage nanoparticle
PFA	paraformaldehyde
P. jirovecii	*Pneumocystis jirovecii*
RI	refractive index
ROR-γt	retinoic acid-related orphan receptor γ t
SDS	sodium dodecyl sulphate
SLO	secondary lymphoid organ
SPIM	selective plane illumination microscopy
S. suis	*Streptococcus suis*
TAMRA	carboxytertamethylrhodamine
TDE	thiodethanol
THF	tetrahydrofurane
Th	T helper
Thy	thymocyte differentiation antigen
THB	Todd Hewitt broth
TLO	tertiary lymphoid organ
TLR	toll-like receptor

TRIF	TIR-domain-containing adaptor-inducing interferon beta
WT	wild type

List of figures

Summary

Induction of bronchus-associated lymphoid tissue by common zoonotic microorganisms, and establishment of a method for its quantification in whole lung lobes

David Mzinza

Bronchus-associated lymphoid tissue (BALT) plays a key role in initiating and maintaining host protective immunity against invading pathogens. It is not constitutively found in most species but can be induced when the lung is exposed to different microorganisms or compounds that cause lung inflammation. Studies from our group describe the induction of BALT by modified vaccinia virus Ankara (MVA), and *Pseudomonas aeruginosa* (*P. aeruginosa*) in mice [1,2]. BALT induced by MVA is characterized by the expression of C-X-C chemokine ligand 12 and 13 (CXCL12 and CXCL13); while in *P. aeruginosa* BALT only CXCL12 is present. In addition, influenza virus, and *Pneumocystis jirovecii* (*P. jirovecii*) have also been shown to induce BALT [3,4]. Here, they attribute the formation of BALT through molecular mechanisms that are driven by T helper 17 (Th17) responses.

From these results we learn that the development of microorganism-induced BALT is driven by different molecular mechanisms. Two pathways have been identified so far. Whereas one pathways rely on the presence of IL-17 (for example *P. aeruginosa*), the second is completely independent of IL-17 (for example MVA). To further understand the development and function of BALT, additional studies, that characterize its induction by other microorganisms, are needed.

So far, BALT is primarily investigated by immunohistology but this approach might not reflect the composition of BALT in the entire lung since only a limited number of sections can be analyzed. Additional approaches to study BALT in the entire lung are urgently needed. Therefore, I set out to develop a method that allows analysis of BALT in the entire lung.

During my doctoral studies, I investigated the induction of BALT by *Escherichia coli* (*E. coli*), *Listeria monocytogenes* (*L. monocytogenes*) and *Streptococcus suis* (*S. suis*). These microorganisms were heat inactivated, before being administered into mice intranasally. Formation of BALT was assessed by histological examination of lung cryosections stained by lymphocyte-specific antibodies. Out of the three microorganisms above, only *E. coli* could induce BALT which is characterized by the presence of organized B cell follicles accompanied by T cells, follicular dendritic cells (FDCs) expressing CXCL13 as well as other CXCL12-expressing stromal cells. This presentation of BALT by *E. coli*, regarding chemokine expression, is like results from MVA-induction model, but different from *P. aeruginosa*, as described above.

I also established the application of light sheet microscopy (LiSM) for the analysis of BALT in whole lung lobes. BALT within lobes was identified by antibody-staining of its constituent T and B cell aggregates. Prior to imaging, lobes were optically cleared in order to match the refractive index (RI) of the lobes with that of the imaging solvent, Dibenzyl ether (DBE). I achieved this by using a protocol that was previously described by *Ertürk et al.* in 2012, called three-dimensional imaging of solvent-cleared organs (3DISCO) which can be used to clear different specimens. Thereafter, cleared lung lobes were imaged by LiSM and BALT was analyzed by Imaris software. Using this approach, I could nicely show the lung's

bronchial tree, the organization and volume of BALT as well as lymphocyte distribution within the entire lobes from uninfected or BALT-bearing mice. Interestingly, when using mice lacking the chemokine receptor CXCR5 *E. coli*-induced BALT is dominated by T cell aggregates. Furthermore, I performed LiSM to visualize the lymphatics distribution within lung lobes using Thy1/CD90 as a suitable marker for murine lung lymph vessels.

This is the first study that describes the induction of BALT by a single intranasal dose of *E. coli* and identifies chemokines and chemokine receptors involved in this process. These results help to understand *E. coli*-specific immune responses and might contribute to the development of further strategies to control its associated infections. Moreover, the application of LiSM on whole lung lobes provides essential new insights in lung architecture as well as in understanding the development and organization of lymphoid aggregates within the whole lung, under different conditions.

Zusammenfassung

Die Induktion von bronchus-assoziiertem lymphatischem Gewebe durch zoonotische Mikroorganismen und die Etablierung einer Methode für dessen Analyse innerhalb kompletter Lungenflügel

David Mzinza

Das bronchus-assoziierte lymphatische Gewebe (BALT) ist Teil eines ausgedehnten lymphatischen Netzwerks, welches das Atmungsepithel und andere Schleimhäute vor eindringenden Pathogenen schützt. Sowohl die Ursachen, die zur Entwicklung dieser Strukturen führen als auch ihre immunologischen Funktionen sind gegenwärtig nur unzureichend geklärt. Bei Wildtyp (WT) Mäusen kommt es normalerweise nicht vor, kann aber durch aerogene Infektion verschiedener respiratorischer Pathogene wie zum Beispiel Modifiziertes Virus Ankara (MVA), *Pseudomonas aeruginosa* (*P. aeruginosa*), Influenza und *Pneumocystis jirovecii* (*P. jirovecii*) induziert werden [1–4]. Die BALT-induzierenden Pathogene bestimmen hierbei welche Mechanismen und Zellpopulationen zur Entwicklung des BALT notwendig sind. In MVA-induziertem BALT differenzieren lokale Stromazellen zu CXCL13-produzierenden follikulären dendritischen Zellen (FDCs), welche B Zellen rekrutieren und die Bildung von B Zellfollikeln fördern. Während diese in *P. aeruginosa*-induziertem BALT fehlen, werden B Zellen hier durch ein anderes Chemokin, CXCL12, rekrutiert. Entscheidend für die Bildung und Aufrechterhaltung der B Zellfollikel in BALT induziert durch *P. aeruginosa,* Influenza und *P. jirovecii* BALT ist das Interleukin-17 (IL-17). Bei der Entwicklung von MVA-induziertem BALT spielt IL-17 hingegen keine Rolle. Diese Studien unterstreichen die Notwendigkeit BALT pathogen-spezifisch zu untersuchen, da sich durch die einzigartigen molekularen Eigenschaften

jedes einzelnen Pathogens Unterschiede in den Entwicklungsmechanismen ergeben können.

Aus diesem Grund wurden in dieser Arbeit die Entwicklung von BALT durch unterschiedliche zoonotische Erreger, wie *Escherichia coli* (*E. coli*), *Listeria monocytogenes* und *Streptococcus suis* untersucht. Von den genannten Erregern führt nur die intranasale Verabreichung von *E. coli* zur Entwicklung von BALT mit organisierten B Zellfollikeln, die sowohl CXCL13-expremierende FDCs als auch andere Stromazellen, die CXCL12 produzieren beinhalten. Wird der CXCL13-CXCR5 Signalweg unterbunden, dominieren interessanterweise T Zellen das induzierte BALT, was auf eine entscheidende Rolle dieses Chemokin/Chemokinrezeptorpaars während der Rekrutierung von B Zellen und der Aufrechterhaltung der B Zellfollikeln hindeutet.

Desweiteren wurde in dieser Arbeit ein Verfahren etabliert, welches die Analyse kompletter Lungenflügel und darin enthaltener lymphatischer Strukturen erlaubt. Die sogenannte *Lightsheet*-Mikroskopie (LiSM) ermöglicht nach entsprechender Antikörperfärbung und optischem *Clearing* der Probe die dreidimensionale Visualisierung des Bronchialsystems der Lunge sowie die Darstellung und Quantifizierung einzelner BALT Strukturen innerhalb kompletter Lungenflügel. Hierzu werden die Lungenflügel vor dem Imaging nach einem kürzlich beschrieben Protokoll (3DISCO: *three-dimensional imaging of solvent-cleared organs*; Ertürk et al., 2012) bis zur Transparenz geklärt, in einer mit Dibenzylether gefüllten Kammer mikroskopiert und anschließend mit einer Analysesoftware ausgewertet. In dieser Arbeit zeigt sich eindrucksvoll, dass sich dieses Verfahren sowohl zur Analyse der Organisation von spontanem und pathogen-induziertem BALT als auch zur Berechnung des gesamten BALT Volumens in WT und

Knockout-Mäusen eignet und gleichzeitig Ergebnisse der konventionellen Immunhistologie bestätigt. Außerdem wurden erste Versuche zur spezifischen Färbung von lymphatischen Gefäßen in der Lunge mittels LiSM durchgeführt. Hierbei wurde Thy1/CD90 als geeigneter Marker identifiziert und erfolgreich zur dreidimensionalen Darstellung von Lymphgefäßen eingesetzt.

Zusammenfassend stellt das hier entwickelte, neuartige Mikroskopie-Verfahren in Kombination mit konventionellen Mikroskopiemethoden eine exzellente Möglichkeit dar, die Entwicklung und Organisation lymphatischer Strukturen und Gefäße in der kompletten Lunge dreidimensional darzustellen und zu quantifizieren. In dieser Studie angewendet, konnte diese Technik bereits wesentliche Erkenntnisse zur *E. coli*-induzierten BALT Entwicklung liefern, welche für zukünftige Behandlungsstrategien gegen von *E. coli* hervorgerufene Infektionen von Bedeutung sein können.

1. Introduction

1.1 Bronchus-associated lymphoid tissue (BALT)

1.1.1 Definition of BALT

Lymphoid organs are important sites for development and induction of host immune responses to invading pathogens[5]. They are classified into 3 types namely, primary, secondary or tertiary lymphoid organs. Primary and secondary lymphoid organs develop during embryogenesis, independent of antigen or inflammatory stimuli, and form in specific anatomical locations[6,7]. Primary lymphoid organs which include thymus and bone marrow act as sites for immune cells development[8], while secondary lymphoid organs (SLOs) such as lymph nodes, spleen and mucosal associated lymphoid tissues are niches for immune cells activation[7]. In contrast, exposure to different pathogens or various forms of immunomodulation can result in the formation of tertiary lymphoid organs (TLOs)[9]. TLOs develop in different organs, including the lung, in which case they are called bronchus-associated lymphoid tissue (BALT).

BALT was first described in pigs and rabbits, as organized mucosal lymphoid follicles located between the bronchial epithelium and pulmonary arteries[10–13]. The cellular organization in BALT was characterized as being similar to other lymphoid tissues like Peyer's patches in the gastrointestinal tract, and nasal-associated lymphoid tissue (NALT) by forming lymphoid follicles underneath an epithelium dome[12,14,15]. BALT commonly develops in spaces that are filled with pulmonary vessels located in parallel to the bronchial airways, because during inflammation these spaces are often filled with lymphocytes[16]. To be classified as BALT, lymphoid aggregates must be located in

association with a bronchus, contain B cell follicles, often organized by the presence of a network of stroma cells such as follicular dendritic cells (FDCs), and surrounded by T cell zones[16,17]. In addition, mature BALT is also characterized by the presence of high endothelial venules (HEVs) as well as lymphatics which facilitate the continuous exchange of immune cells[16]. The cellular composition and organization of BALT is portrayed in **Figure 1**.

1.1.2 Organization of cells in BALT

BALT is mostly composed of B cell follicles that are mostly populated by B cells expressing immunoglobulins A, D and M (IgA, IgD and IgM)[18,19]. In addition macrophages[20], dendritic cells (DCs)[1,21] as well as $CD4^+$ T cells[22] may also be found within the B cell follicles. Macrophages and DCs might be involved in antigen presentation and also clearance of apoptotic B cells[23], while $CD4^+$ T cells facilitate germinal center reactions[24]. FDCs are also prominently found within B cell follicles. Their major role is to express chemokines, such as C-X-C chemokine ligand 13 (CXCL13) which interacts with its receptor C-X-C receptor 5 (CXCR5) that is expressed on B cells[25]. This interaction facilitates the recruitment, organization and maintenance of B cell follicles[26]. In cases where plasma cells are present, they are commonly located around the edges of B cell follicles or within the T cell zones[27].

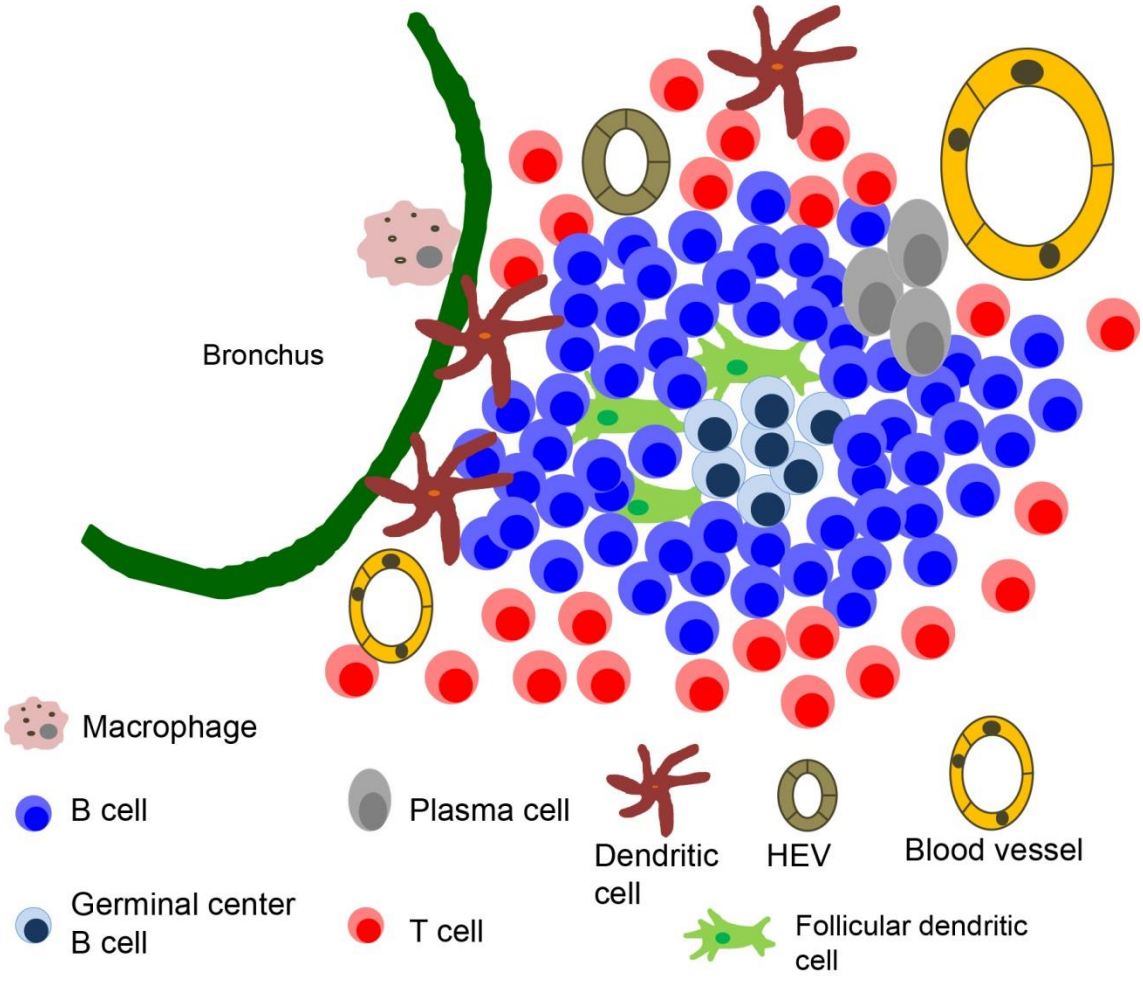

Figure 1: Cellular organization in BALT. BALT forms near airways and surrounding blood vessels. B cell follicles are commonly located centrally, within which FDCs can also be found. DCs are mostly located within the T cell zones that in most cases surround B cell follicles. Within BALT, HEVs, plasma cells and germinal centers can also be found[28].

T cells in BALT are mostly positioned around or in between B cell follicles[22]. In most cases, unlike B cells, they do not form organized aggregates but are highly populated by fibroblastic reticular like cells that express C-C chemokine ligand 19 and 21 (CCL19, CCL19)[29–31]. These 2 chemokines recruit T cells by interacting with C-C chemokine

receptor 7 (CCR7) that is expressed by T cells[25,32]. In addition, DCs[22], macrophages[33] and plasma cells[27] can also be found within T cell zones. HEVs, which in SLOs are conduits through which naïve T cells are recruited[30], and also lymphatic vessels[3,34] can often be found within T cell zones or at the border with B cell follicles[16]. It remains unclear whether these roles are also similar for BALT and other TLOs.

1.1.3 Formation of BALT

The development of BALT is supported by chemokine-driven reactions. These chemokines include CXCL12 and CXCL13 which are responsible for B cell recruitment[35,36], as well as CCL19 and CCL21 which recruit T cells[37,38]. Lymphotoxin (LT), which is produced by lymphoid tissue inducer (LTi) cells[39], upregulates the expression of CXCL13, CCL19 and CCL21 chemokines[40]. Mice deficient of inhibiter of differentiation 2 (Id2) and retinoic acid-related orphan receptor γ t (ROR-γt), which are transcriptional factors involved in the differentiation of LTi cells[41], develop influenza virus-induced BALT in mice[3,42]. This clearly shows that the development of BALT might not entirely depend on LTi cells, but their role in upregulating lymphocyte recruitment chemokines cannot be overlooked. Furthermore, it is interesting to note that when these cells are adoptively transferred in the skin, they have been shown to induce the formation of TLOs[43]. Therefore, it remains important to study LTi and their association with the development of BALT.

Furthermore, during BALT development, the expression of CXCL13 and CCL19 can be modulated by other cytokines, including IL-17. In influenza virus BALT induction model for instance, neonatal mice challenged with LPS highly expressed CXCL13, IL-17 and IL-

23p19 compared to adult mice treated similarly. Later in life when these mice were challenged with influenza virus, only those treated with LPS during neonatal stage developed BALT[35]. These findings suggested that the accumulation of IL-17 producing cells within the lung, partly enhanced by the presence of IL-23[44], and promoted the development of BALT. In contrast, influenza virus-induced BALT is impaired in mice deficient of IL-17A, IL-23p23 and IL-17RA[35]. Recent studies have shown that the development of *P. aeruginosa*-induced BALT also depends on the presence of IL-17 producing cells. Here, in the presence of IL-17, stroma cells differentiate and express CXCL12 which mediated formation of B cell follicles[36].

Induced BALT does not develop through programmed events involving specific cells and chemokines, unlike other lymphoid organs. Not all chemokines mentioned above are necessarily involved in the formation of BALT. For instance, *Ccr7*$^{-/-}$ mice develop spontaneous BALT[18], in which case there is no involvement of CCL19 or CCL21 associated signaling. More important, events that drive the formation of BALT could be specific to the induction stimulus. Below, several BALT-induction models are discussed.

1.1.4 Induction models to study the development and organization of BALT

To date, BALT has been described in many species including rats[45,46], mice[1,4,35,36], guinea pig[46], cats[47] as well as human beings[34,48]. Unlike secondary lymphoid organs, BALT is not constitutively available in most of these species, but rather can be induced by pulmonary exposure to various microorganisms or different forms of lung inflammation. In mice, viral and bacterial induction models have been described, among them including MVA[1,36], *P.*

aeruginosa[36], influenza virus[35] and recently in a fungus-model, using *Pneumocystis jirovecii*[4].

Administration of a single dose of the non-replicating MVA is enough to induce BALT formation in mice, maintained by the presence of DCs and characterized by the presence of FDCs and expression of CXCL12 and CXCL13[1,36]. Following MVA administration, mice clear the virus and develop organized BALT peaking around 12 days following viral administration[1]. From further work in our group, another microorganism in which induction of BALT has been described is *P. aeruginosa*[36,49]. Unlike MVA, *P. aeruginosa*-induced BALT is characterized by the expression of CXCL12 only, and to induce BALT 2 doses are required – with the second dose given 6 days following the first one[36].

Several studies from the lab of Troy Randall characterizing the induction of BALT by influenza virus have been reported. They postulate that influenza virus-induced BALT is dependent on the expression of CXCL13, CCL19 and CCL21 which are all triggered by IL-17[35], and that its maintenance requires lymphotoxin α (LTα)[27,35]. In addition to viruses and bacteria, *P. jirovecii* is the first fungal microorganism that has been described to induce BALT in mice. In a recent study by Eddens, *et al.* it was observed that an infection of mice with *P. jirovecii* led to the induction of CXCL13 and formation of BALT[4]. These authors further demonstrated that BALT formation in this model is dependent of the expression of CXCL13, which is induced by Th2 or Th17 reponses[4].

It is clear from the above examples that different molecules and pathways are necessary for BALT development and maintenance in different induction models. In all induction models described above, the role of chemokines seems to be inevitable for BALT formation and maintenance. Therefore, if we are to fully understand the development and

maintenance of BALT, it is necessary to conduct more studies on its induction by different microorganisms.

1.1.5 Role of BALT in induction of host protective immune responses

Secondary lymphoid organs play a significant role in the induction of host protective immune responses by providing a niche where naïve lymphocytes can get activated, differentiated and proliferate in response to specific invading pathogens. Lymphocyte activation is driven by the arrival of mature antigen presenting cells which come loaded with antigens. The structure and cellular organization of BALT is similar to secondary lymphoid organs, therefore, their role in induction of host protective immune responses are similar, as observed below.

The role of BALT in providing host protective immune responses were first described in LT-deficient mice which have a defect in the development of conventional lymphoid organs. Even though in these mice the development of conventional lymphoid organs is impaired[3,50], they were able to mount protective immune responses by successfully generating T and B cell responses capable of clearing pulmonary influenza virus thereby sustaining their survival[3]. In that study, the authors were also able to demonstrate that BALT supports proliferation of CD4 and CD8 positive T cells[3].

DCs are not only essential in maintaining the organization of BALT, but they also interact with and prime naive T cells within BALT, making it a general site for T cell priming[1]. Here, mice with MVA-induced BALT received antigen-specific and polyclonal T cells, together with mature DCs, 24 hours later. Only antigen-specific T cells were able to interact with transferred DCs, while no such interactions were observed for polyclonal T cells[1].

More evidence to show the role of BALT in induction of protective immune response was reported against *Mycobacterium tuberculosis* (MTB). Here, Day *et al.* demonstrated that protective immune responses specific for MTB were generated following granuloma formation in mice lacking SLOs[51]. Surprisingly, gene expression analyses revealed upregulation of genes associated with formation of lymphoid organs, including CXCL13, CCL19, CXCR5, CCR7, LTα and LTβ, suggesting that the formation of pulmonary granulomas might follow programs similar to the development of lymphoid organs[51]. The presence of granulomas and BALT provided control against MTB infection in these mice, in the absence of conventional lymphoid organs.

1.1.6 Visualization and analysis of BALT using immunohistology

To study the development and organization of BALT, immunohistology has been the main method used until now. This method involves preparation of lung cryosections, antibody staining followed by fluorescence microscopy, to determine the formation of BALT and perform further analyses. Immunohistology is a well-established method but it has several limitations. We now know from spontaneous BALT in CCR7-deficient mice is commonly located in the region close to the main bronchi and surrounding vessels[18], and analysis of lung cryosections from within this region can be representative for the entire lung, with minimal differences from one section to another. Histological analysis by nature is limited, since only few sections can be analyzed per lung.

In an intranasal application model, depending on the animals breathing, BALT-inducing microorganisms can be deposited elsewhere along the lung bronchial tree, and not only

always along the main bronchi and surrounding vessels. Thus, a more accurate way of BALT quantification would be the analysis of BALT in complete lungs.

1.2 Light sheet microscopy (LiSM)

1.2.1 LiSM set up

The first light sheet microscope, referred to as ultramicroscopy, was described in the early 20th century by Siedentopf and Zsigmondy who at that time were employed by Carl Zeiss to manufacture optical systems[52]. By projecting sunlight through a slit aperture, they were able to study and determine the size of colloidal nanoparticles in gold ruby glass[52,53]. In the following years, the use of light sheet microscopy was primarily for chemistry and materials science analyses, until in the early 1990s when investigators from the lab of Francis Spelman developed an improved light sheet system which they called orthogonal plane fluorescence and optical sectioning (OPFOS), in their attempt to quantitatively assess cochlear features using experiments in guinea pigs[53,54]. However, within the last decade, numerous advances aiming at developing the method further and exploration of novel applications have been reported, earning its recognition as the method of the year in 2014, by Nature Methods journal[55].

Several microscopy techniques, including confocal and 2-photon imaging, can be optimised for use to analyse thick specimen sections. However, unlike these approaches, LiSM is designed so that the specimen is illuminated from the side to minimize excitation of fluorophores outside the illuminated plane[56,57] **(Figure 2A)**. In this case, the exposed region is limited to a thin plane while the fluorescence of the entire field of view gets detected with substantial reduction in photo bleaching as well as blurriness from out of

focus regions[56–59] **(Figure 2B)**. Combined with computational analyses, LiSM produces data that is well registered and can suitably be used for 3-dimensional (3D) reconstruction of imaged specimens, providing substantial advances regarding the understanding of different biological systems[57].

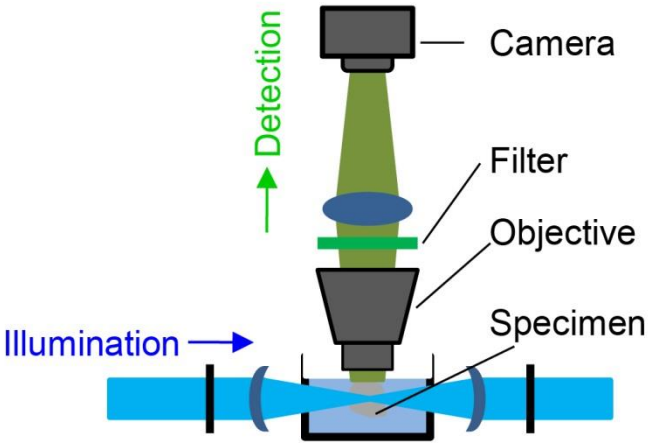

Figure 2: LiSM optics set up. The specimen is illuminated from the side, along the focal plane, by a thin sheet of laser light. The specimen is then imaged by an objective lens and individual images from each focal plane are captured by a camera, along the detection direction. Specimen illumination with a thin sheet of laser light overlapping the focal plane ensures that photo bleaching is minimized during imaging. *Illustration inspired by Becker et al, 2013*[60].

There are two ways in which a light sheet can be generated. The first option is to allow the laser to pass through a cylindrical lens thereby turning the incoming beam into a thin light sheet[61]. This approach has been widely adopted and generally used in selective plane illumination microscopy (SPIM)[62]. Alternatively, a thin light sheet can be generated by scanning a micron-thin laser rapidly in the vertical direction through the specimen when it is exposed[56]. The illumination efficiency when using this approach is highly improved

because there is no requirement for beam-shaping units[56]. This option is commonly referred to as digitally scanned light sheet based fluorescence microscopy (DSLM)[63]. During LiSM imaging, the generation of a thin light sheet is based on the arrangement similar to SPIM[59].

1.2.2 Specimen optical clearing

Imaging of thick tissues and whole organs is challenging because during this process light is directed through several cellular and extracellular structures which possess different refractive indices (RIs) resulting into scattering of light[64]. Due to the scattering of light, acquired images from such specimens are of very low quality and the imaging depth is usually rather restricted. To overcome this limitation, specimens have to be optically cleared to match their RIs to that of the imaging medium. This process reduces light scattering during image acquisition thereby improving the overall quality of images and imaging depth. Different optical clearing protocols, each one designed to suit specific imaging requirements, have been developed. Here the most commonly used, which are (1) clear, unobstructed brain/body imaging cocktails and computational analysis (CUBIC)[65], (2) clear lipid-exchange Acrylamide-hybridised rigid imaging/ immunostaining/in-situ-hybridisation-compatible tissue hydrogel (CLARITY) and (3) three-dimensional imaging of solvent-cleared organs(3DISCO)[64], will be discussed in detail.

CUBIC was originally developed to study brain samples, but it has also been applied for specimens from other organs[66,67]. For optical clearing using this protocol, specimens are incubated in two different reagent mixtures (reagent-1 and reagent-2). Reagent-1 is made of a mixture of (Ethylenedidnitrilo) tetra 2- propanol, Triton X-100 and urea, while reagent-

2 is a mixture of triethanolamine, urea and sucrose[65]. CUBIC uses water soluble reagents which preserve fluorescence, making it an ideal protocol for optical clearing of organs prepared from transgenic animals that express specific fluorescent proteins.

Like CUBIC, CLARITY is also based on incubation of specimens in mixtures of aqueous solutions, making it also best suited for organs expressing transgenic immunofluorescent proteins. Optical clearing using this protocol is achieved through perfusion of specimens with a mixture of a fixative and a cocktail of hydrogel monomers. Specimens are then polymerized by heating and cleared by incubation in Boric acid[68–70]. Clearing time can relatively longer depending on the organ, but it can be shortened by electrophoresis[71].

3DISCO, unlike either CUBIC or CLARITY, is designed to use organic solvents. Here specimens are dehydrated first before elimination of lipids and subsequent clearing of the dehydrated specimen. Specimen dehydration is achieved by incubation in increasing concentrations of Tetrahydrofurane (THF), and thereafter cleared in Dibenzyl ether (DBE)[64]. In alternative organic solvent based clearing protocols, methanol with or without hexane can be used for specimen dehydration, while Benzyl Benzoate, Dichloromethane, Benzyl alcohol or Methylsalicilate can be used for clearing[72]. The original 3DISCO optical clearing protocol is optimized for imaging antibody-stained specimens because DBE is known to quench fluorescent proteins, and also toxic[73,74]. However, recently there have been improvements to the protocol in which DBE can be replaced by other solvents such as Ethyl-3-phenylprop-2-enoate (Ethyl Cinnamate) which is commonly used as a food additive and in cosmetic products[75,76].

1.3 Study objectives

1.3.1 Investigation of BALT by common zoonotic microorganisms

BALT plays a role in induction of host protective immune responses; therefore, it is important to understand its development and organization under different conditions. Previous work from our group have described the development and function of MVA-induced BALT[1,36,77], as well as the development and organization of *P. aeruginosa*-induced BALT[36]. Recent findings from our group indicate that BALT development occurs following different molecular pathways depending on the inducing microorganism. This was demonstrated through studying and comparing key cells, cytokines and chemokines involved in development of MVA- and *P. aeruginosa*-induced BALT. Until now, there have been opposing findings regarding the necessity of certain cells, chemokines and cytokines that are required in the formation and maintenance of BALT; therefore, it is important to do more studies on microorganism-specific BALT.

Therefore, in the current study I wanted to screen and investigate more microorganisms for their ability to induce BALT and to comparatively study BALT formation induced by different pathogens. Three different zoonotic microorganisms that are known to be associated with respiratory or mucosal infections were selected for this purpose. These microorganisms included *L. monocytogenes*, *S. suis* and *E. coli*. BALT induction was investigated using immunohistology, as well as LiSM in an *E. coli*-induction model.

1.3.2 Visualization and quantitative analysis of BALT in whole lung lobes

Until now, analysis of BALT has been done mainly using immunohistology of thin lung cryosections. In previous studies from our group it was observed that spontaneous BALT

in *Ccr7*$^{-/-}$ mice is commonly located close to the main bronchi and surrounding vessels[18]. To make investigation of BALT more accurate, time-saving and vivid I aimed to develop semi-automatic imaging and analysis of whole lung lobes. Therefore, I established a LiSM protocol for optical clearing and imaging of entire lung lobes as well as subsequent quantification of BALT in those lungs. To establish this method, I used lung lobes from *Ccr7*$^{-/-}$ mice, that contained spontaneous BALT, as well as lobes from mice in which BALT was induced by administration of MVA or *E. coli*. I used antibody staining as well as adoptive cell transfers to identify and quantify BALT by using Imaris image analysis software.

2. Materials and methods

Detailed materials and methods that were used for results that have been submitted for peer reviewed publication are not described in this section, because they already appear in the manuscript (see section 3.1.2).

Propagation and preparation of all the bacteria used in my experiments was done in Prof. Dr. Peter Valentin-Weigand laboratory (Institute for Microbiology, University of Veterinary Medicine Hannover, Hannover, Germany). MVA was kindly provided by Prof. Dr. Gerd Sutter (Institute of Infection Medicine and Zoonoses, University of Munich LMU, Munich Germany). *Myd88/Trif*$^{-/-}$*, Myd88/Trif/Cardif*$^{-/-}$*,* and *Ifnar1*$^{-/-}$ mice were kindly provided by Prof. Dr. Ulrich Kalinke (TWINCORE, Centre for Experimental and Clinical Infection Research, Hannover, Germany).

2.1 Microorganisms

2.1.1 *L. monocytogenes*

L. monocytogenes was streaked on Columbia agar with sheep red blood (Oxoid), followed by incubation overnight at 37^{o}C in the incubator. One colony was inoculated into 100ml BHI-Bouillon medium, in a conical flask, and incubated overnight at 37^{o}C in an incubator. Bacteria were then pelleted (by centrifugation at 2100xg for 10 minutes), washed once and re-suspended in PBS. CFUs were determined by plating different dilutions and direct counting using a Thoma cell counting chamber. Before they were used in experiments, bacteria were heat inactivated, by autoclaving or incubations in a water bath. Heat inactivation was confirmed by plating the autoclaved material on Columbia agar and incubation at 37^{o}C for 72 hours.

2.1.2 *S. suis* strain 10

Bacteria were streaked out, on Columbia agar with sheep red blood (Oxoid) and incubated overnight at 37ºC in an incubator. Single colonies were inoculated into 10ml of THB-Bouillon medium in a 14ml Greiner-Tube and incubated overnight at 37ºC in an ice bath to prevent bacterial overgrowth. Cultures were then diluted 1:200 in 500ml THB-Bouillon medium in a chicane flask, without shaking, after which they were grown up to OD_{600} (OD was determined using a BioPhotometer). Bacteria were then pelleted by centrifugation (2100xg for 10 minutes), washed once and re-suspended in PBS. CFUs were determined by plating different dilutions and direct counting using a Thoma cell counting chamber. Inactivation of the bacteria was achieved by either autoclaving or incubations in a water bath. Heat inactivation was confirmed by plating the autoclaved material on Columbia agar followed by incubation at 37ºC for 72 hours.

2.2 LiSM

2.2.1 Dye/antibody lung perfusion

Immediately after mice were sacrificed, the lung was perfused with 10ml PBS, followed by 5 ml 4% PFA solution. Thereafter, it was slowly perfused with Tomato lectin DyLight 594 dye, anti-Lyve-1, or anti-MECA-32 antibodies and left to incubate for at least 10 to 15 minutes. Afterwards, the lung was filled with 4% PFA, isolated and incubated in a similar concentration of PFA (3ml) for further 2 hours.

2.2.1 Optical clearing (CLARITY)

A similar protocol to the one described for studies of rat brain development was used[70]. Briefly, immediately after being sacrificed the lungs of mice were perfused with 10ml PBS supplemented with 4% PFA, 4% Acrylamide, and 0.25% VA-044 initiator. To improve the structural integrity of the lung lobes, 2% Acrolein was used. Lobes were fixed overnight at 4^{o}C, after which they were incubated for 3 hours in a water bath to allow polymerization. Optical clearing was done by incubating the lung lobes in a mixture of 0.2M Boric acid and 2% Sodium dodecyl sulphate (SDS) for at least 6 days or until they developed a transparent appearance. RI matching was done by incubating the lobes in 20%, 40% and 60% 2, 20-Thiodethanol (TDE) solution for at least 4 hours each. Cleared lung lobes were imaged in 60% TDE.

3. Results

3.1 Publication

Application of light sheet microscopy for qualitative and quantitative analysis of bronchus-associated lymphoid tissue in mice

Mzinza DT, Fleige H, Laarmann K, Willenzon S, Ristenpart J, Spanier J, Sutter G, Kalinke U, Valentin-Weigand P, Förster R.

Cell Mol Immunol. 2018 Feb 12. doi: 10.1038/cmi.2017.150. [Epub ahead of print]

Contribution: performed ~90% and analyzed all *E. coli* BALT induction experiments, analyzed all MVA BALT induction experiments, performed and analyzed all LiSM related experiments, and wrote the first draft of the manuscript.

Abstract

Bronchus-associated lymphoid tissue (BALT) develops at unpredictable locations around lung bronchi following pulmonary inflammation. The formation and composition of BALT is mostly investigated by immunohistology that, due to the size of the invested organ, is usually restricted to few histological sections. To assess the entire BALT of a lung other approaches are urgently needed. Here we introduce a novel light sheet microscopy-based approach of assessing lymphoid tissue in the lung. Using antibody staining of whole lung lobes and optical clearing by organic solvents we present a method that allows in depth visualization of the entire bronchial tree, the lymphatic vasculature as well as the immune

cell composition of the induced BALT. Furthermore, a three-dimensional analysis of the entire lung allows to qualitatively and quantitatively enumerate the induced BALT, therein. Using this approach, we show that in contrast to wild type mice (WT), a single intranasal application of the replication-deficient poxvirus MVA induces BALT that adds up to 8% of the entire lung volume in mice deficient for the CCR7. Furthermore, BALT induced by heat inactivated *E. coli* is dominated by pronounced T cell infiltration in *Cxcr5*-deficient but not in WT mice.

3.2 BALT induction by common zoonotic microorganisms

In further experiments, I investigated the induction of BALT by *L. monocytogenes* and *S. suis* in mice. *L. monocytogenes* is predominantly a gut associated pathogen; *S. suis* can colonize the respiratory tract. More important, both microorganisms are mucosal tissue-associated and also zoonotic. All of them can be transmitted from animals to humans through consumption of food products from infected livestock.

L. monocytogenes is well known gram-positive bacteria and is one of the major food-borne pathogen causing listeriosis disease in both humans and animals. It can be transmitted from animals to humans through consumption of contaminated food products ranging from meats, seafood, milk products or vegetables. It tends to infect the host macrophages where it can survive and multiply. To regain their phagocytic ability, macrophages require the presence of IFN-γ which is produced mostly by T cells driven by pro-inflammatory cytokines secreted by infected the macrophages[78]. Host neutrophils can also provide immunity against *L. monocytogenes* through the generation of extracellular traps with granule-derived proteins and chromatin to trap the bacteria, in addition to releasing chemokines such as monocyte chemoattractant protein-1 (MCP-1) which recruits more macrophages to the site of infection. Even though *L. monocytogenes* is not a common resident of the respiratory system, it contributes to lung infections such as pneumonia especially in the elderly population[79,80].

S. suis is also a gram-positive bacteria that is commonly associated with a wide range of infections, mainly in pigs including septicemia, meningitis, pneumonia, endocarditis, and arthritis[81–83]. It is a highly diverse microorganism consisting up to 35 serotypes that have been identified based on antigens found on its capsular polysaccharide (CPS); serotype

2 is the most frequently reported worldwide and is commonly associated with infections in pigs as well as humans[83,84]. In addition to causing major economic losses in the swine industry, *S. suis* associated infections in humans have been reported, most of them occurring in south eastern Asia and other regions with extensive swine farming[85]. It can be transmitted from pigs to humans through contact with *S. suis* contaminated animals or carcasses, for whom, in addition to meningitis, in humans, *S. suis* can also cause pneumonia as well as different forms of systemic infections affecting many organs[84,85]. The pathogenicity of *S. suis* is reinforced by a large display of virulent factors, of which the most important ones include CPS, hemolysin, extracellular factor (EF), muraminidase released protein (MRP), enzymes and adhensins[86,87]. The host immune system, through the epithelium cell layer, can control the progression of *S. suis* by constant secretion of mucus and cilia-mediated sweeping away the bacteria. Like many other bacterial infections, phagocytes play a significant role in eliminating any of the *S. suis* that can breach the epithelial barrier. However, the presence of the CPS and ability to produce hemolysin enables it to escape phagocytosis by avoiding the complement system[88,89].

3.2.1 Mice administered with *L. monocytogenes* develop lymphoid aggregates

In the first experiment set up, 6 to 8 weeks old WT mice were intranasally administered with 3 different concentrations of autoclaved *L. monocytogenes* to determine the optimal bacterial concentration. These were 10^7 CFU/ml, $5x10^7$ CFU/ml or 10^8 CFU/ml per mouse. To determine the formation of BALT, lungs from these mice were isolated and analyzed 12 days later following bacterial administration, by immunohistology of cryosections.

Results from these experiments revealed the formation of isolated cellular infiltrates, some of which were close to the bronchus **(Figure 3A)**. Further analyses were done by staining cryosections with anti-CD3 and anti-B220 antibodies to determine the frequency of lymphocyte populations within these infiltrates. Indeed, this staining revealed the presence of both T and B cells **(Figure 3B)**. Despite the case that these infiltrates were composed of B cell aggregates, they were very few per section and none of them could be classified as BALT because they lacked organized B cell follicles. In separate experiments, an additional second intranasal dose (10^8 CFU/ml) of autoclaved *L. monocytogenes* was given 6 days after the first one, however, it did not lead to formation in higher numbers or organization of the induced infiltrates **(Figure 3C)**. Again, T and B cells could be detected in the infiltrates, but almost all infiltrates were highly dominated by T cells with very few B cells **(Figure 3D)**.

With the assumption that autoclaving might lead to the loss of most of the bacteria's pathogen-associated molecular patterns (PAMPs), we decided to mildly heat-inactivate *L. monocytogenes* by incubating at 85^{o}C for 15 minutes so as to preserve the PAMPs. Therefore, we administered one dose, 10^8 CFU/ml, of the mildly inactivated bacteria in mice and analyzed the formation of BALT as before. However, unlike results from the previous experiments, I did not find formation of any cellular infiltrations **(Figure 4E)**. Similarly, when 2 doses were given as in the previous experiment set up, no formation of cellular infiltrates was observed (data not shown).

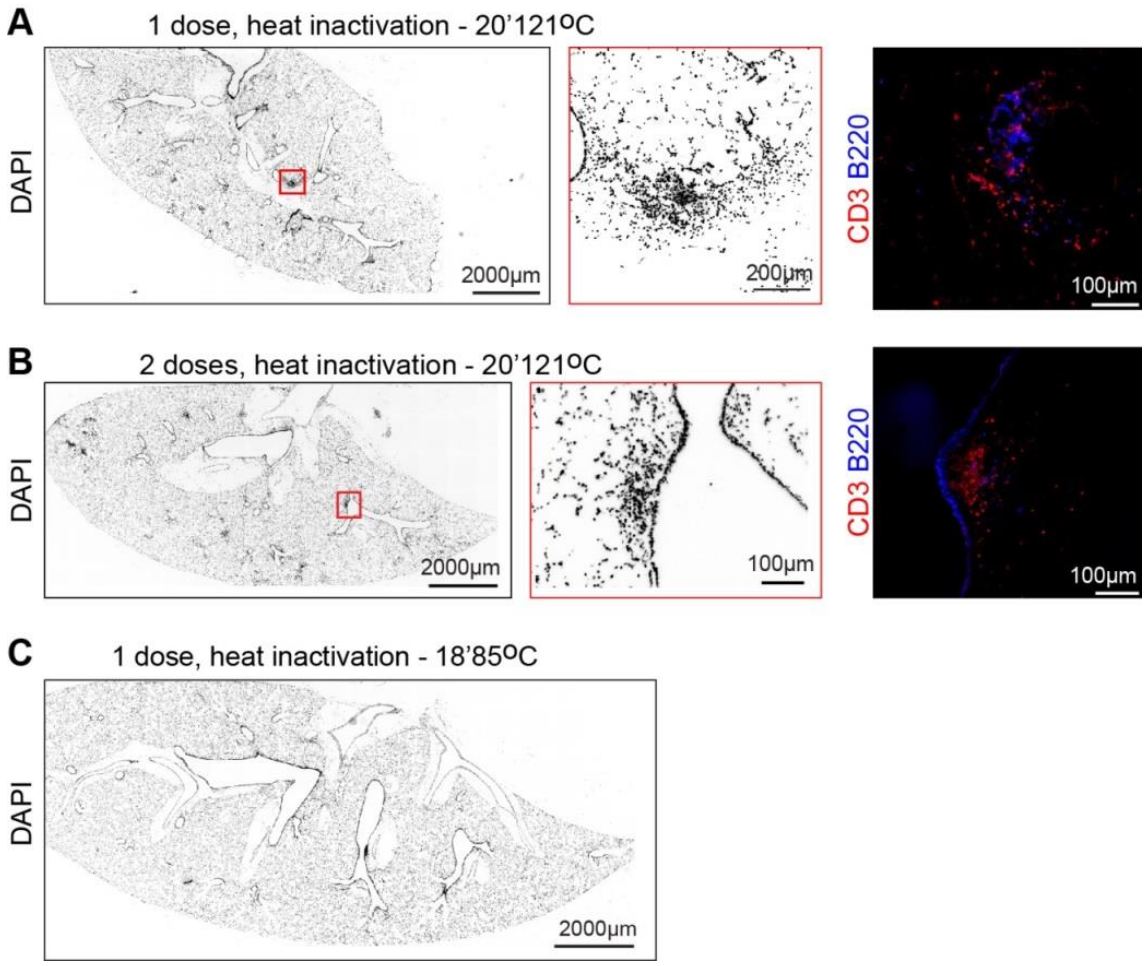

Figure 3: Mice administered with *L. monocytogenes* develop cellular infiltrations and lymphoid aggregates in their lungs. **(A)** Representative micrographs from lung sections following administration of a single dose of autoclaved *L. monocytogenes*. **(B)** Representative micrographs from lung sections following administration of 2 doses of autoclaved *L. monocytogenes*. The second dose was administered 6 days after the first one. **(C)** Representative micrographs from lung sections following administration of a single dose of mildly inactivated *L. monocytogenes*. Cryosections were stained with DAPI dye, anti-CD3 and anti-B220 antibodies.

From the above experiments, it was clear that intranasal administration of *L. monocytogenes* can induce the formation of cellular infiltrations in which both T and B

cells are present. However, these cell infiltrates were very few, and could not be described as BALT because they lacked organization of B cell follicles.

3.2.2 Mice administered with *S. suis* develop unorganized lymphoid aggregates

Likewise, I investigated if the administration of *S. suis* in mice would induce the formation of BALT. These experiments were also done in 6 to 8 weeks old WT mice, initially by intranasal administration of different concentrations ($4x10^7$ CFU/ml, $2x10^8$ CFU/ml and 10^9 CFU/ml). To determine the formation of BALT, lungs from these mice were isolated and analyzed as described for *L. monocytogenes* above.

Results revealed the formation of isolated cellular infiltrates in mice administered with either $4x10^7$ CFU/ml or $2x10^8$ CFU/ml like those observed in *L. monocytogenes* experiments. However, slightly more infiltrates formed in mice administered with a higher dose (10^9) of bacteria **(Figure 4A)**. Nevertheless, these infiltrates contained both T and B cells, in unorganized formations **(Figure 4B)** located close to the bronchus. To analyze whether an additional bacterial dose leads to more and higher organized infiltrates, in a second experiment set up, a second dose (10^9 CFU/ml) of *S. suis* was administered on day 6 from the first dose.

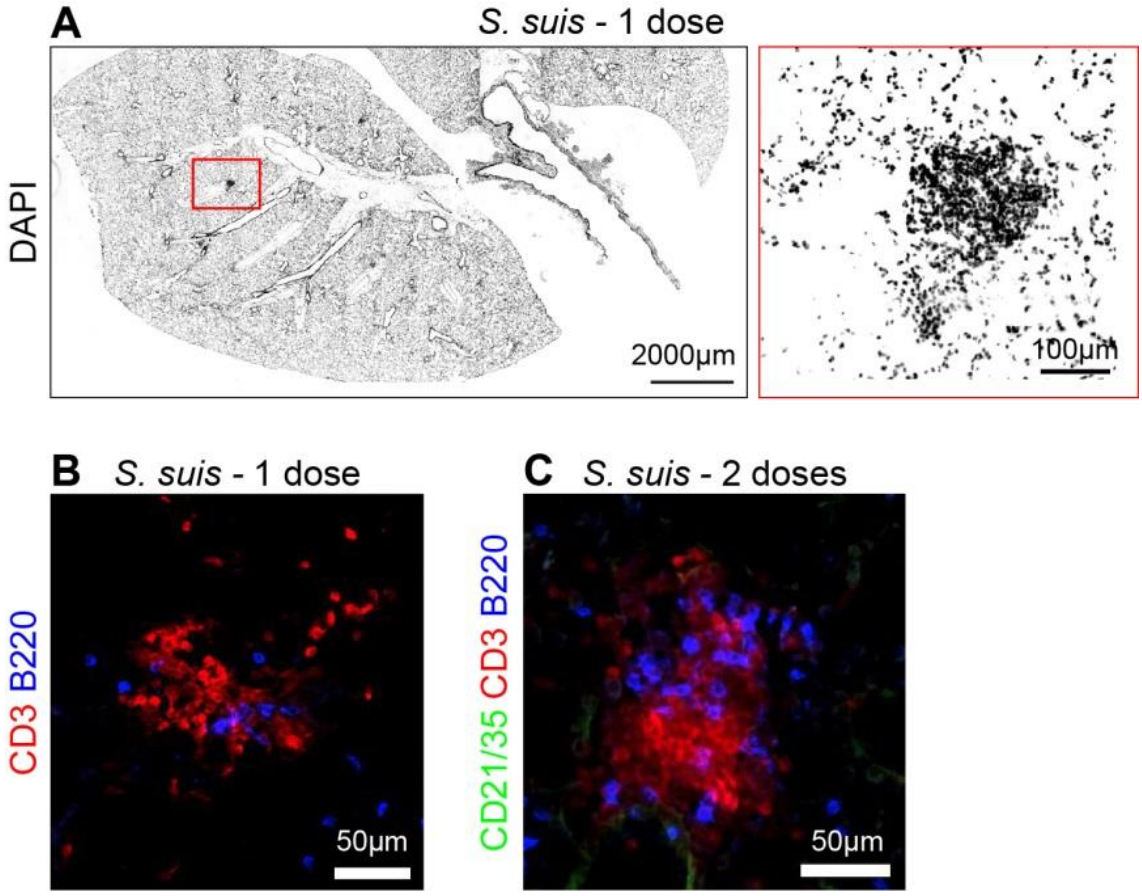

Figure 4: Mice that are administered with *S. suis* develop organized lymphoid aggregates, but not characteristic of BALT. **(A)** Representative lung micrographs taken from lung cryosection from mice after administration of a single dose of *S. suis*. **(B)** Representative micrograph taken from lung cryosections of mice administered with a single dose of *S. suis*. Cryosections were stained with anti-CD3 and anti-B220 antibodies. **(C)** Representative micrograph taken from mice administered with 2 doses of *S. suis*. The second dose was administered 6 days after the first. In all cases lung cryosections were stained with DAPI, anti-CD21/35, anti-CD and/or anti-B220 antibodies.

Here the mice also developed cellular aggregates characterized by more T cell zones and unorganized B cells **(Figure 4C)**. The organization of the aggregates was not much

different when compared to the experiment set up in which only one dose was administered, however in the current set up, T cells dominated in most of the aggregates.

In additional experiments, mice were administered with *S. suis* that was inactivated by either incubating the bacteria at 50^{o}C for 40 minutes or two incubations of 50^{o}C for 30 minutes plus 85^{o}C for 15 minutes. This was done to ensure the PAMPs from the bacteria were preserved, which might not be the case with autoclaving. However, from these experiments I could not find and cellular infiltration from lungs of these mice.

According to results from the experiments above, it therefore seems possible to conclude that intranasal administration of heat-inactivated *S. suis* induces the formation of lymphoid aggregates that are populated by both T and B cells in the lungs of mice. However, the aggregates are rather not organized to be characterized as BALT.

In the above experiments, it was determined whether intranasal administration of either *L. monocytogenes* or *S. suis* can induce the formation of BALT in mice. Different experiment set ups were followed, including administration of either a single or 2 doses of the microorganisms as well as administration of microorganisms that have been heat-inactivated differently. In all cases formation of either cellular infiltrates or unorganized lymphoid aggregates, where both T and B cells were present, could be identified. However, none of them were characteristic of BALT.

3.3 Visualization of vessels in LiSM imaged lung lobes

In addition to the application of LiSM imaging for the analysis of BALT, in this study I also attempted to show the distribution of blood and lymphatic vessels within lung lobes. Previous reports have showed that BALT is associated with both blood and

lymphatic vessels, as well as HEVs[16]. These vessels can be seen in micrographs taken from antibody stained thin lung cryosections. Their presentation is mostly limited to 2D visualization it is challenging to envisage the entire interactions. Before imaging the association of BALT and vessels, it was necessary to first determine the ability to label and visualize vessels in mouse lung lobes, using LiSM.

We therefore stained whole lung lobes from uninfected WT mice with anti-Thy-1 for the detection of lymphatic vessels, and Tomato lectin dye, anti-Lyve-1 and anti-MECA-32 antibodies for the identification of blood vessels[90–92]. For staining of blood vessels, dye/antibodies were perfused directly into the lung. Lung lobes with antibody stained vessels were then optically cleared using 3DISCO protocol, and imaged on a light sheet microscope, as in the previous experiments above.

Starting with visualization of blood vessels, I tested if lung perfusion of the anti-Lyve-1, anti-MECA-32 or Tomato lectin dye was optimal to label and visualize them using LiSM. Here immediately after sacrificing the mice, the lung was perfused with either of the above antibodies/dye followed by PFA fixation and LiSM imaging thereafter. In both cases blood vessels could be identified. However, in lung lobes that were perfused with anti-Lyve-1 or anti-MECA-32 antibodies the staining was more prominent for small vessels and capillaries within the lobe's parenchyma **(Figure 5A and B)**. In contrast, for lung lobes that were perfused with Tomato lectin dye it was possible to label bigger vessels in addition to smaller ones and capillaries **(Figure 5C and E)**.

For the identification of lymphatic vessels, lung lobes were stained with anti-Thy1.2 antibody. Briefly, after PFA fixation and non-specific binding blocking by incubation in

PBS with serum, lung lobes were incubated in anti-Thy1.2 antibody diluted in PBS. After 72 hours of incubation, the lobes were optically cleared using 3DISCO protocol and imaged on a light sheet microscope. Results showed successful staining of vessels **(Figure 5D)**, which were determined to be lymphatic vessels because Thy1.2 antibody has been shown to be specific for lymphatic vessels in the lung[90,93].

After successfully identification of blood and lymphatic vessels, using Tomato lectin lung perfusion and Thy1.2 antibody respectively, in the next experiment I intended to use these two staining together. Here the lung lobes were first perfused with Tomato lectin dye followed by Thy1.2 staining, all done as in previous experiments outlined above. Again, here it was possible to see all the vessels **(Figure 5E)**; however, the Tomato lectin staining was not as prominent as when in the case where it was used alone. This was the case most likely because of several washes that followed Thy1.2 staining.

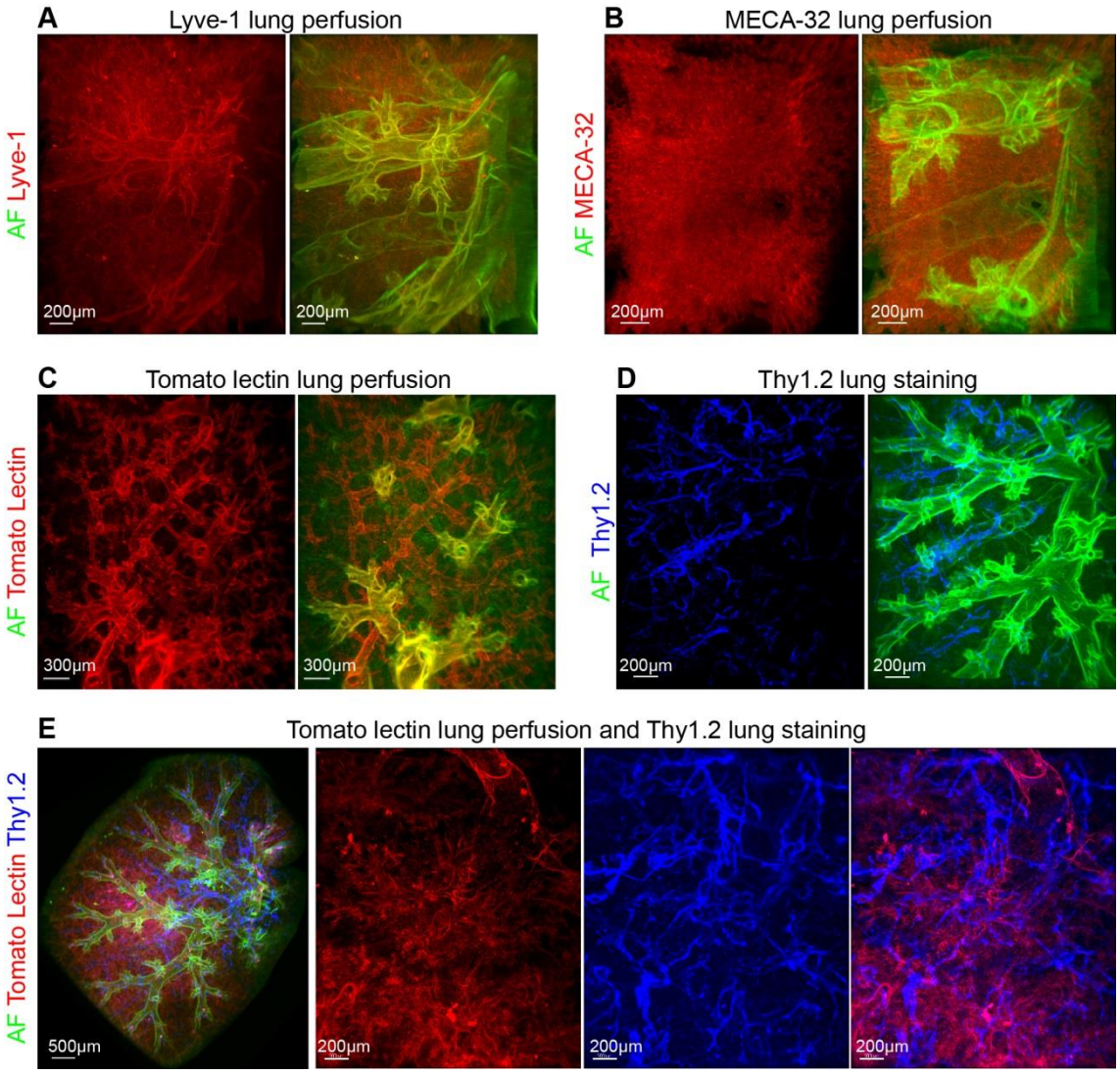

Figure 5: Visualization of blood and lymphatic vessels in LiSM imaged lung lobes. Representative lung lobe micrographs showing blood and lymphatic vessels following **(A)** Lyve-1 lung perfusion, **(B)** MECA-32 lung perfusion, **(C)** Tomato lectin lung perfusion and **(D)** Thy1.2 staining. **(E)** Representative lung lobe micrograph showing Tomato lectin lung perfusion and co-staining with Thy1.2 antibody. Green represents autofluorescence (AF).

In the above experiments, I could show that LiSM can be successfully adopted for visualization of additional structures within entire lung lobes. Tomato lectin lung perfusion

was identified as a better option for labelling blood vessels compared to either Lyve-1 or MECA-32 antibodies. Its combination with Thy1.2 was adequate to visualize both blood and lymphatic vessels. Further work on these experiments would be to analyze and track the anatomy of blood and lymphatic vessels directly connected to BALT.

4. Discussion

4.1 *E. coli*: a new candidate for induction of BALT

In this study, I identified that *E. coli* can induce organized lymphoid aggregates which are characteristic of BALT. A single intranasal administration of heat-inactivated *E. coli* could induce BALT that was characterized by organized B cell follicles surrounded by T cells, FDCs and other stromal cells expressing the chemokines CXCL13 and CXCL12. The two chemokines, however, were expressed at different time points of BALT development. BALT development was detectable from day 6, peaking on day 18 and remaining the same up to day 30 following *E. coli* administration. CXCL12 expression was present at all analysis time points, while CXCL13 was only detectable from day 18 onwards. It was not surprising that the expression of CXCL13 coincided with the emergence of FDCs, since these cells are its main producer[26]. It appears that the formation of *E. coli*-induced BALT might be similar to that induced by MVA induction, where CXCL13 played a major role in organizing the follicles[2]. However, the main difference is that, the peak time point in the development of MVA-induced BALT is day 12[1], while for *E. coli* it is day 18.

To further characterize the role of CXCL13 in the development of *E. coli*-induced BALT, I tested the effect of its organization in mice that are deficient for the CXCL13 receptor, CXCR5. Results from these experiments revealed that B cell follicles were arranged differently when compared to results from WT mice. Indeed, CXCL13 in addition to recruitment of B cells in lymphoid organs is also responsible for organizing them therein. This has already been observed in mice where the disruption of CXCR5 leads to defects in the migration and organization of B cell follicles within conventional lymphoid organs[94]. Regarding TLOs, in addition to my observations in *E. coli* BALT organization, a similar

defect in the organization of B cell follicles has been recently reported in *P. jirovecii*-induced BALT[4]. Moreover, I found that the absence of CXCR5 did not affect the number of induced aggregates in total, but rather the frequency of classical BALT (type I aggregates). Rather, in these mice the frequency of type II aggregates was higher, and further results from LiSM images revealed that most aggregates were dominated by T cells. Along the same line, *Cxcr5*-deficieny does not interfere with the frequency[2] but equally with the organization of MVA-induced BALT (unpublished data). Similar observations have also been made by Rangel-Moreno and colleagues showing that the loss of CXCL13 had minimal impact on either the development or function of influenza-induced BALT[95]

Recent results from our group indicate that the combined lack of TLR signaling adaptor molecules (MyD88 and TRIF) impairs the development of *P. aeruginosa*-induced BALT[2]. Surprisingly, I could now show that this is not the case for BALT induced by *E. coli*. Mice deficient of either 2 (MyD88 and TRIF) or 3 (MyD88, TRIF and Cardif) adaptor molecules do not reveal a detectable difference in induction or organization of BALT compared to WT mice. MyD88 is regarded as a general signaling adaptor molecule associated with TLRs. However, for TLR4, MyD88-independent signaling pathways which are triggered by LPS have been previously reported[96]. The role of *E. coli* LPS has not been addressed in the current experiments, but it is known that in neonatal mice that have been exposed to LPS are capable of developing influenza virus-induced BALT later in life[35]. Based on these previous observations, it is therefore fair to speculate that the formation of *E. coli*-induced BALT in mice lacking either 2 or 3 of the adaptor molecules described above might be dependent on other pathways that do not involve MyD88. Since Cardif is

commonly associated with signaling resulting into antiviral immune responses[97,98], I did not expect that its absence would have an effect on *E. coli*.

Interestingly, in contrast to the above mentioned TLR adaptors, the absence of type I IFN signaling slightly impairs BALT induction by *E. coli*. Even though BALT development was possible in *Ifnar1*-deficient mice, the frequency was reduced, and induced B cell follicles frequently lacked FDCs compared to results from WT mice. Type I IFNs signal by inducing of viral nucleic acids and proteins acting on TLRs[99], hence in similarity with Cardif, they are mostly associated with anti-viral responses. Since IFN signaling is known to contribute to protective immunity against *E. coli* infection by enhancing the production of pro-inflammatory cytokines[100], it can be speculated that in the current experiments the impairment of BALT development in *Ifnar1*-deficient mice might be attributed to the induction of protective immunity against *E. coli*.

On the contrary, other zoonotic pathogens that have been tested in this study, such as *L. monocytogenes* and *S. suis,* did not induce the formation of BALT in WT mice. Not all microorganisms are capable to induce the formation of BALT. Unlike secondary lymphoid organs, the formation of BALT and other TLOs do not follow a genetically encoded chain of events. Rather their development and maintenance is determined by the invading pathogen and how the host's immune system responds to it. *L. monocytogenes* is able to escape from phagocytosis by disrupting the phagosome membrane in a manner mediated by listeriolysin and phospholipase[101]. Likewise, *S. suis* can easily escape innate immunity by secreting toxins that make them resistant to innate immunity[88,102,103].

4.2 LiSM application opens more possibilities for analysis of BALT

In addition to investigate the induction of BALT by common zoonotic microorganisms, in this study I also present first-time data showing the application of LiSM for qualitative and quantitative analysis of BALT in whole lung lobes. To date, LiSM has been applied for the study of structures in different organs in mice including brain[104], spinal cord[105,106], kidneys[75], embryos[107] and also human specimens[108].

This novel method has recently been advanced by the establishment of several optical clearing protocols. The choice of which protocol to use depends on the type of specimen and the experimental set up. Of the two commonly applied clearing protocols, CLARITY[70] and 3DISCO[64], the latter was found to be more suited for the lung regarding imaging and analysis of the whole lung lobes. Unlike CLARITY, 3DISCO required much shorter time for sample preparation prior to imaging, facilitated excellent imaging depth of cleared samples, and enhanced the handling of lung lobes (dehydrated lobes had a better integrity for handling during imaging).

Furthermore, I could show that antibody staining enables labelling BALT within whole lung lobes. Since the majority of cells in BALT are T and B cells[16] those cells were targeted by antibody staining to identify BALT by LiSM. Using the 3DISCO protocol for clearing of antibody stained specimens[64,73], it was possible to visualize and analyze spontaneous and induced BALT in entire lung lobes of mice. The general location of spontaneous BALT in *Ccr7*$^{-/-}$ mice, as described by previous work from our group[18], has been a key guide for the analysis of any form of BALT until now. Based on these observations, the analysis of cryosections from within the region of the main bronchus has been accepted as a standard representation of the entire lung.

Immunohistology remains the best method for analyzing the cellular composition and distribution within BALT, however, due to technical-caused differences in the distribution of induced BALT throughout the lung, reliance on immunohistology analyses alone might result into higher variations. During intranasal administration of microorganisms, it is not possible to determine its spread in different lobes. The mice are prone to sneezing out the microorganisms, and even though this can be avoided by deep anesthesia, the internal spread might still depend on the mouse's breathing.

LiSM provides an additional essential approach, because here it is possible to image and view all BALT within the entire lung lobes. Combining LiSM and existing methods like immunohistology helped to understand the organization of *E. coli*-induced lymphoid aggregates in *Cxcr5*$^{-/-}$ mice. Performing immunohistology of representative cryosections I could determine that the lungs from these mice were dominated by type II lymphoid aggregates, which is interestingly different from what we had previously shown for MVA and *P. aeruginosa*[36] in which at the peak time point all aggregates were dominantly type I. This observation was confirmed by LiSM that overall, most aggregates were dominated by unorganized aggregates with the majority being T cells. Furthermore, LiSM together with computational analysis enabled measurement of the volume of the lung lobe occupied by BALT as well as the distribution of individual cellular aggregates. Even though it is possible to physically section the thick specimens and determine reconstruct 3D images from series of 2D collected per section[109,110], this approach is rather labor intensive, and difficult to maintain quality of the sections.

Ongoing work is now focused on trying to determine the anatomy of blood and lymphatic vessels and how they are connected to BALT. In preliminary results, I could show that

blood and lymphatic vessels can be stained by the perfusion of labelled Tomato lectin followed by Thy-1 antibody staining. Lectins are proteins that are different from antibodies in that they are capable of binding carbohydrate components on endothelial cells along vascular tissues[111]. They have been used to label and visualize blood vessels in mouse brain and different other organs through their transfer by circulation[112,113]. Similarly, Thy-1 antibody has been previously shown to specifically stain lymphatic endothelial cells in the lung[90]. However, experiments will be needed to improve the imaging resolution, for example by combining LiSM and 2-photon microscopy.

4.3 Concluding remarks

Mature antigen-presenting cells from the lung normally are required to migrate and induce protective immune responses in lung draining lymph nodes. The presence of induced BALT within the lung, providing a niche for protective immune response induction, can be viewed as important sites for enhancing local immunity against various respiratory pathogens. Even though, the immune responses generated from within BALT might be delayed (i.e. these responses wait until BALT develop - this may take several days to weeks), manipulation of induced BALT could prove to be useful in furthering targeted control of infections. An example of such an approach is described in the study by Wiley et al. in which they propose a strategy to utilize protein cage nanoparticle (PCN) to accelerate the clearance of respiratory viruses[114].

In this project I found out that *E. coli* is capable of inducing the formation of BALT in mice. Even though I was able to show similarity in the key molecules for its formation and maintenance to the ones described for MVA, more studies are necessary. For instance,

in this study I could not determine what virulence factors were responsible for BALT induction. Future studies should therefore be focused on determining the possibility of inducing BALT by different *E. coli* PAMPs. Furthermore, the application of LiSM in analysis of BALT is a great advancement tool that can additionally be used to further describe BALT in different models. Using this method, I could determine the BALT volume in entire lung lobes, as well as volumes of lymphocyte aggregates and lung lobes by conducting manual analyses. With additional computational analysis performed on LiSM imaged lung lobes it is also possible to determine more features of BALT. For example, the institution of automated algorithm for the analysis BALT and associated features in LiSM images could provide endless possibilities towards the advancement of our knowledge of BALT.

5. References

1 Halle S, Dujardin HC, Bakocevic N, Fleige H, Danzer H, Willenzon S *et al.* Induced bronchus-associated lymphoid tissue serves as a general priming site for T cells and is maintained by dendritic cells. *J Exp Med* 2009; **206**: 2593–601.

2 Fleige H, Ravens S, Moschovakis GL, Bolter J, Willenzon S, Sutter G *et al.* IL-17-induced CXCL12 recruits B cells and induces follicle formation in BALT in the absence of differentiated FDCs. *J Exp Med* 2014; **211**: 643–651.

3 Moyron-Quiroz JE, Rangel-Moreno J, Kusser K, Hartson L, Sprague F, Goodrich S *et al.* Role of inducible bronchus associated lymphoid tissue (iBALT) in respiratory immunity. *Nat Med* 2004; **10**: 927–34.

4 Eddens T, Elsegeiny W, Garcia-Hernadez M de la L, Castillo P, Trevejo-Nunez G, Serody K *et al.* Pneumocystis-Driven Inducible Bronchus-Associated Lymphoid Tissue Formation Requires Th2 and Th17 Immunity. *Cell Rep* 2017; **18**: 3078–3090.

5 Chaplin DD. Overview of the immune response. *J Allergy Clin Immunol* 2010; **125**: S3-23.

6 Randall TD, Carragher DM, Rangel-Moreno J. Development of secondary lymphoid organs. *Annu Rev Immunol* 2008; **26**: 627–650.

7 Drayton DL, Liao S, Mounzer RH, Ruddle NH. Lymphoid organ development: from ontogeny to neogenesis. *Nat Immunol* 2006; **7**: 344–353.

8 Anderson G, Takahama Y. Thymic epithelial cells: working class heroes for T cell development and repertoire selection. *Trends Immunol* 2012; **33**: 256–263.

9 Jones GW, Hill DG, Jones SA. Understanding Immune Cells in Tertiary Lymphoid Organ Development: It Is All Starting to Come Together. *Front Immunol* 2016; **7**: 401.

10 Bienenstock J, Johnston N, Perey DY. Bronchial lymphoid tissue. II. Functional characterisitics. *Lab Invest* 1973; **28**: 693–698.

11 Bienenstock J, Johnston N, Perey DY. Bronchial lymphoid tissue. I. Morphologic characteristics. *Lab Invest* 1973; **28**: 686–92.

12 Bienenstock J, Johnston N. A morphologic study of rabbit bronchial lymphoid aggregates and lymphoepithelium. *Lab Invest* 1976; **35**: 343–348.

13 Gehrke I, Pabst R. The epithelium overlying rabbit bronchus-associated lymphoid tissue does not express the secretory component of immunoglobulin A. *Cell Tissue Res* 1990; **259**: 397–9.

14 Sminia T, van der Brugge-Gamelkoorn GJ, Jeurissen SH. Structure and function of bronchus-associated lymphoid tissue (BALT). *Crit Rev Immunol* 1989; **9**: 119–50.

15 Kiyono H, Fukuyama S. NALT- versus Peyer's-patch-mediated mucosal immunity. *Nat Rev Immunol* 2004; **4**: 699–710.

16 Randall TD. Bronchus-associated lymphoid tissue (BALT) structure and function. *Adv Immunol* 2010; **107**: 187–241.

17 Pabst R. Plasticity and heterogeneity of lymphoid organs. *Immunol Lett* 2007; **112**: 1–8.

18 Kocks JR, Davalos-Misslitz ACM, Hintzen G, Ohl L, Förster R. Regulatory T cells interfere with the development of bronchus-associated lymphoid tissue. *J Exp Med* 2007; **204**: 723–34.

19 Otsuki Y, Ito Y, Magari S. Lymphocyte subpopulations in high endothelial venules and lymphatic capillaries of bronchus-associated lymphoid tissue (BALT) in the rat. *Am J Anat* 1989; **184**: 139–46.

20 Van Der Brugge-Gamelkoorn GJ, Dijkstra CD, Sminia T. Characterization of pulmonary macrophages and bronchus-associated lymphoid tissue (BALT) macrophages in the rat. An enzyme-cytochemical and immunocytochemical study. *Immunobiology* 1985; **169**: 553–62.

21 Moyron-Quiroz JE, Rangel-Moreno J, Hartson L, Kusser K, Tighe MP, Klonowski KD *et al.* Persistence and responsiveness of immunologic memory in the absence of secondary lymphoid organs. *Immunity* 2006; **25**: 643–54.

22 Woodland DL, Randall TD. Anatomical features of anti-viral immunity in the respiratory tract. *Semin Immunol* 2004; **16**: 163–170.

23 Randall TD. *Structure, Organisation, and development of the mucosal immune system of the respiratory tract*. Elsevier, 2015 doi:10.1016/B978-0-12-415847-4.00004-5.

24 Vinuesa CG, Tangye SG, Moser B, Mackay CR. Follicular B helper T cells in antibody responses and autoimmunity. *Nat Rev Immunol* 2005; **5**: 853–865.

25 Schulz O, Hammerschmidt SI, Moschovakis GL, Förster R. Chemokines and Chemokine Receptors in Lymphoid Tissue Dynamics. *Annu Rev Immunol* 2016. doi:10.1146/annurev-immunol-041015-055649.

26 Cyster JG, Ansel KM, Ngo VN, Hyman PL, Luther SA, Förster R *et al.* A chemokine-driven positive feedback loop organizes lymphoid follicles. *Nature* 2000; **406**: 309–314.

27 GeurtsvanKessel CH, Willart MAM, Bergen IM, van Rijt LS, Muskens F, Elewaut D *et al.* Dendritic cells are crucial for maintenance of tertiary lymphoid structures in the lung of influenza virus-infected mice. *J Exp Med* 2009; **206**: 2339–49.

28 Randall TD. Pulmonary dendritic cells: thinking globally, acting locally. *J Exp Med* 2010; **207**: 451–454.

29 Link A, Vogt TK, Favre S, Britschgi MR, Acha-Orbea H, Hinz B *et al.* Fibroblastic reticular cells in lymph nodes regulate the homeostasis of naive T cells. *Nat Immunol* 2007; **8**: 1255–65.

30 Link A, Hardie DL, Favre S, Britschgi MR, Adams DH, Sixt M *et al.* Association of T-zone reticular networks and conduits with ectopic lymphoid tissues in mice and humans. *Am J Pathol* 2011; **178**: 1662–75.

31 Barone F, Gardner DH, Nayar S, Steinthal N, Buckley CD, Luther SA. Stromal fibroblasts in tertiary lymphoid structures: A novel target in chronic inflammation. Front. Immunol. 2016; **7**: 477.

32 Förster R, Pabst O, Bernhardt G. Homeostatic chemokines in development, plasticity, and

functional organization of the intestinal immune system. *Semin Immunol* 2008; **20**: 171–180.

33 Hiramatsu K, Azuma A, Kudoh S, Desaki M, Takizawa H, Sugawara I. Inhalation of diesel exhaust for three months affects major cytokine expression and induces bronchus-associated lymphoid tissue formation in murine lungs. *Exp Lung Res* 2003; **29**: 607–22.

34 Rangel-Moreno J, Hartson L, Navarro C, Gaxiola M, Selman M, Randall TD. Inducible bronchus-associated lymphoid tissue (iBALT) in patients with pulmonary complications of rheumatoid arthritis. *J Clin Invest* 2006; **116**: 3183–94.

35 Rangel-Moreno J, Carragher DM, de la Luz Garcia-Hernandez M, Hwang JY, Kusser K, Hartson L *et al.* The development of inducible bronchus-associated lymphoid tissue depends on IL-17. *Nat Immunol* 2011; **12**: 639–46.

36 Fleige H, Ravens S, Moschovakis GL, Bölter J, Willenzon S, Sutter G *et al.* IL-17-induced CXCL12 recruits B cells and induces follicle formation in BALT in the absence of differentiated FDCs. *J Exp Med* 2014; **211**: 643–51.

37 Cyster JG. Chemokines and Cell Migration in Secondary Lymphoid Organs. *Science (80-)* 1999; **286**: 2098–2102.

38 Förster R, Schubel A, Breitfeld D, Kremmer E, Renner-Müller I, Wolf E *et al.* CCR7 coordinates the primary immune response by establishing functional microenvironments in secondary lymphoid organs. *Cell* 1999; **99**: 23–33.

39 Mebius RE, Rennert P, Weissman IL. Developing lymph nodes collect CD4+CD3- LTbeta+ cells that can differentiate to APC, NK cells, and follicular cells but not T or B cells. *Immunity* 1997; **7**: 493–504.

40 Randall TD, Mebius RE. The development and function of mucosal lymphoid tissues: a balancing act with micro-organisms. *Mucosal Immunol* 2014; **7**: 455–66.

41 Cherrier M, Sawa S, Eberl G. Notch, Id2, and RORγt sequentially orchestrate the fetal development of lymphoid tissue inducer cells. *J Exp Med* 2012; **209**: 729–40.

42 Lochner M, Ohnmacht C, Presley L, Bruhns P, Si-Tahar M, Sawa S *et al.* Microbiota-induced tertiary lymphoid tissues aggravate inflammatory disease in the absence of RORγt and LTi cells. *J Exp Med* 2011; **208**: 125–34.

43 Cupedo T, Jansen W, Kraal G, Mebius RE. Induction of secondary and tertiary lymphoid structures in the skin. *Immunity* 2004; **21**: 655–667.

44 Zhou L, Ivanov II, Spolski R, Min R, Shenderov K, Egawa T *et al.* IL-6 programs T(H)-17 cell differentiation by promoting sequential engagement of the IL-21 and IL-23 pathways. *Nat Immunol* 2007; **8**: 967–974.

45 Lührmann A, Tschernig T, Pabst R. Stimulation of bronchus-associated lymphoid tissue in rats by repeated inhalation of aerosolized lipopeptide MALP-2. *Pathobiology* 2002; **70**: 266–9.

46 van der Brugge-Gamelkoorn GJ, Kraal G. The specificity of the high endothelial venule in bronchus-associated lymphoid tissue (BALT). *J Immunol* 1985; **134**: 3746–50.

47 Ms A-T, Wa K. Light Microscopy of Bronchial Associated Lymphoid Tissue of Healthy Domestic Cat with Suggested New Nomenclature. *Anat Physiol* 2012; **2**: 2–5.

48 Tschernig T, Pabst R. Bronchus-associated lymphoid tissue (BALT) is not present in the normal adult lung but in different diseases. *Pathobiology* 2000; **68**: 1–8.

49 Toyoshima M, Chida K, Sato A. Antigen uptake and subsequent cell kinetics in bronchus-associated lymphoid tissue. *Respirology* 2000; **5**: 141–5.

50 De Togni P, Goellner J, Ruddle NH, Streeter PR, Fick A, Mariathasan S *et al.* Abnormal development of peripheral lymphoid organs in mice deficient in lymphotoxin. *Science* 1994; **264**: 703–707.

51 Day TA, Koch M, Nouailles G, Jacobsen M, Kosmiadi GA, Miekley D *et al.* Secondary lymphoid organs are dispensable for the development of T-cell-mediated immunity during tuberculosis. *Eur J Immunol* 2010; **40**: 1663–73.

52 Siedentopf H, Zsigmondy R. Uber Sichtbarmachung und Größenbestimmung ultramikoskopischer Teilchen, mit besonderer Anwendung auf Goldrubingläser. *Ann Phys* 1902; **315**: 1–39.

53 Khairy K, Lemon WC, Amat F, Keller PJ. Light sheet-based imaging and analysis of early embryogenesis in the fruit fly. In: *Methods in molecular biology (Clifton, N.J.)*. 2015, pp 79–97.

54 Voie AH, Burns DH, Spelman FA. Orthogonal-plane fluorescence optical sectioning: three-dimensional imaging of macroscopic biological specimens. *J Microsc* 1993; **170**: 229–36.

55 Methods of the year 2014. *Nat Methods* 2015; **12**: 19–38.

56 De Vos WH, Beghuin D, Schwarz CJ, Jones DB, van Loon JJWA, Bereiter-Hahn J *et al.* Invited Review Article: Advanced light microscopy for biological space research. *Rev Sci Instrum* 2014; **85**: 101101.

57 Santi PA. Light Sheet Fluorescence Microscopy A Review. *J Histochem Cytochem* 2011; **59**: 129–138.

58 Mohan K, Purnapatra SB, Mondal PP. Three dimensional fluorescence imaging using multiple light-sheet microscopy. *PLoS One* 2014; **9**: e96551.

59 Reynaud EG, Krzic U, Greger K, Stelzer EHK. Light sheet-based fluorescence microscopy: more dimensions, more photons, and less photodamage. *HFSP J* 2008; **2**: 266–275.

60 Becker K, Jährling N, Saghafi S, Dodt H-U. Ultramicroscopy: light-sheet-based microscopy for imaging centimeter-sized objects with micrometer resolution. *Cold Spring Harb Protoc* 2013; **2013**: 704–13.

61 Huisken J. Optical Sectioning Deep Inside Live Embryos by Selective Plane Illumination Microscopy. *Science (80-)* 2004; **305**: 1007–1009.

62 Huisken J, Stainier DYR. Selective plane illumination microscopy techniques in developmental biology. *Development* 2009; **136**.http://dev.biologists.org/content/136/12/1963 (accessed 24 May2017).

63 Keller PJ, Schmidt AD, Wittbrodt J, Stelzer EHK. Digital scanned laser light-sheet fluorescence microscopy (DSLM) of zebrafish and Drosophila embryonic development. *Cold Spring Harb Protoc* 2011; **2011**: 1235–43.

64 Ertürk A, Becker K, Jährling N, Mauch CP, Hojer CD, Egen JG *et al.* Three-dimensional imaging of solvent-cleared organs using 3DISCO. *Nat Protoc* 2012; **7**: 1983–95.

65 Susaki EA, Tainaka K, Perrin D, Yukinaga H, Kuno A, Ueda HR. Advanced CUBIC protocols for whole-brain and whole-body clearing and imaging. *Nat Protoc* 2015; **10**: 1709–1727.

66 Susaki EA a., Tainaka K, Perrin D, Kishino F, Tawara T, Watanabe TMM *et al.* Whole-brain imaging with single-cell resolution using chemical cocktails and computational analysis. *Cell* 2014; **157**: 726–739.

67 Tainaka K, Kubota SI, Suyama TQ, Susaki EA, Perrin D, Ukai-Tadenuma M *et al.* Whole-Body Imaging with Single-Cell Resolution by Tissue Decolorization. *Cell* 2014; **159**: 911–924.

68 Tomer R, Ye L, Hsueh B, Deisseroth K. Advanced CLARITY for rapid and high-resolution imaging of intact tissues. *Nat Protoc* 2014; **9**: 1682–97.

69 Costantini I, Ghobril J-P, Di Giovanna AP, Mascaro ALA, Silvestri L, Müllenbroich MC *et al.* A versatile clearing agent for multi-modal brain imaging. *Sci Rep* 2015; **5**: 9808.

70 Zheng H, Rinaman L. Simplified CLARITY for visualizing immunofluorescence labeling in the developing rat brain. *Brain Struct Funct* 2016; **221**: 2375–2383.

71 Epp JR, Niibori Y, Liz Hsiang H-L, Mercaldo V, Deisseroth K, Josselyn SA *et al.* Optimization of CLARITY for Clearing Whole-Brain and Other Intact Organs(1,2,3). *eNeuro*; **2**. doi:10.1523/ENEURO.0022-15.2015.

72 Becker K, Jährling N, Saghafi S, Weiler R, Dodt H-U. Chemical Clearing and Dehydration of GFP Expressing Mouse Brains. *PLoS One* 2012; **7**: e33916.

73 Renier N, Wu Z, Simon DJ, Yang J, Ariel P, Tessier-Lavigne M. iDISCO: A Simple, Rapid Method

to Immunolabel Large Tissue Samples for Volume Imaging. *Cell* 2014; **159**: 896–910.

74 Azaripour A, Lagerweij T, Scharfbillig C, Jadczak AE, Willershausen B, Van Noorden CJF. A survey of clearing techniques for 3D imaging of tissues with special reference to connective tissue. *Prog Histochem Cytochem* 2016. doi:10.1016/j.proghi.2016.04.001.

75 Klingberg A, Hasenberg A, Ludwig-Portugall I, Medyukhina A, Männ L, Brenzel A *et al.* Fully Automated Evaluation of Total Glomerular Number and Capillary Tuft Size in Nephritic Kidneys Using Lightsheet Microscopy. *J Am Soc Nephrol* 2017; **28**: 452–459.

76 Mai L, Xiao L, Huang Y, Mai W. Novel microRNAs involved in regulation of cardiac fi brosis. *Int J Cardiol* 2015; **192**: 14–15.

77 Fleige H, Haas JD, Stahl FR, Willenzon S, Prinz I, Förster R. Induction of BALT in the absence of IL-17. *Nat Immunol* 2012; **13**: 1; author reply 2.

78 Mackaness GB. Cellular resistance to infection. *J Exp Med* 1962; **116**: 381–406.

79 García-Montero M, Rodríguez-García JL, Calvo P, González JM, Fernández-Garrido M, Loza E *et al.* Pneumonia caused by Listeria monocytogenes. *Respiration* 1995; **62**: 107–9.

80 Koufakis T, Chatzopoulou M, Margaritis A, Tsiakalou M, Gabranis I. Pneumonia by Listeria monocytogenes: A Common Infection by an Uncommon Pathogen. *Case Rep Infect Dis* 2015; **2015**: 627073.

81 Staats JJ, Feder I, Okwumabua O, Chengappa MM. Streptococcus suis: Past and present. Vet. Res. Commun. 1997; **21**: 381–407.

82 Gottschalk M, Higgins R, Jacques M, Mittal KR, Henrichsen J. Description of 14 new capsular types of Streptococcus suis. *J Clin Microbiol* 1989; **27**: 2633–2636.

83 Lun Z-R, Wang Q-P, Chen X-G, Li A-X, Zhu X-Q. Streptococcus suis: an emerging zoonotic pathogen. *Lancet Infect Dis* 2007; **7**: 201–209.

84 Gottschalk M, Xu J, Calzas C, Segura M. Streptococcus suis: a new emerging or an old neglected

zoonotic pathogen? *Future Microbiol* 2010; **5**: 371–91.

85 Wertheim HFL, Nghia HDT, Taylor W, Schultsz C. Streptococcus suis: an emerging human pathogen. *Clin Infect Dis* 2009; **48**: 617–25.

86 Fittipaldi N, Segura M, Grenier D, Gottschalk M. Virulence factors involved in the pathogenesis of the infection caused by the swine pathogen and zoonotic agent Streptococcus suis. *Future Microbiol* 2012; **7**: 259–79.

87 Segura M, Calzas C, Grenier D, Gottschalk M. Initial steps of the pathogenesis of the infection caused by Streptococcus suis: fighting against nonspecific defenses. FEBS Lett. 2016; **590**: 3772–3799.

88 Seitz M, Beineke A, Singpiel A, Willenborg J, Dutow P, Goethe R *et al.* Role of capsule and suilysin in mucosal infection of complement-deficient mice with Streptococcus suis. *Infect Immun* 2014; **82**: 2460–71.

89 Brazeau C, Gottschalk M, Vincelette S, Martineau-Doize B. In vitro phagocytosis and survival of Streptococcus suis capsular type 2 inside murine macrophages. *Microbiology* 1996; **142**: 1231–1237.

90 Kretschmer S, Dethlefsen I, Hagner-Benes S, Marsh LM, Garn H, König P. Visualization of intrapulmonary lymph vessels in healthy and inflamed murine lung using CD90/Thy-1 as a marker. *PLoS One* 2013; **8**: e55201.

91 Favre CJ, Mancuso M, Maas K, McLean JW, Baluk P, McDonald DM. Expression of genes involved in vascular development and angiogenesis in endothelial cells of adult lung. *Am J Physiol Circ Physiol* 2003; **285**: H1917–H1938.

92 Sleeman JP, Krishnan J, Kirkin V, Baumann P. Markers for the lymphatic endothelium: In search of the holy grail? *Microsc Res Tech* 2001; **55**: 61–69.

93 Jurisic G. Thymus cell antigen 1 (Thy1, CD90) is expressed by lymphatic vessels and mediates cell adhesion to lymphatic endothelium . *Changes* 2012; **29**: 997–1003.

94 Förster R, Mattis AE, Kremmer E, Wolf E, Brem G, Lipp M. A putative chemokine receptor, BLR1, directs B cell migration to defined lymphoid organs and specific anatomic compartments of the spleen. *Cell* 1996; **87**: 1037–47.

95 Rangel-Moreno J, Moyron-Quiroz JE, Hartson L, Kusser K, Randall TD. Pulmonary expression of CXC chemokine ligand 13, CC chemokine ligand 19, and CC chemokine ligand 21 is essential for local immunity to influenza. *Proc Natl Acad Sci U S A* 2007; **104**: 10577–82.

96 Kawai T, Takeuchi O, Fujita T, Inoue J, Mühlradt PF, Sato S *et al.* Lipopolysaccharide stimulates the MyD88-independent pathway and results in activation of IFN-regulatory factor 3 and the expression of a subset of lipopolysaccharide-inducible genes. *J Immunol* 2001; **167**: 5887–94.

97 Meylan E, Curran J, Hofmann K, Moradpour D, Binder M, Bartenschlager R *et al.* Cardif is an adaptor protein in the RIG-I antiviral pathway and is targeted by hepatitis C virus. *Nature* 2005; **437**: 1167–1172.

98 Delaloye J, Roger T, Steiner-Tardivel QG, Le Roy D, Reymond MK, Akira S *et al.* Innate immune sensing of modified vaccinia virus Ankara (MVA) is mediated by TLR2-TLR6, MDA-5 and the NALP3 inflammasome. *PLoS Pathog* 2009; **5**: e1000480.

99 Welsh RM, Bahl K, Marshall HD, Urban SL. Type 1 interferons and antiviral CD8 T-Cell responses. *PLoS Pathog* 2012; **8**: e1002352.

100 Mancuso G, Midiri A, Biondo C, Beninati C, Zummo S, Galbo R *et al.* Type I IFN Signaling Is Crucial for Host Resistance against Different Species of Pathogenic Bacteria. *J Immunol* 2007; **178**: 3126–3133.

101 Fuchs TM, Eisenreich W, Kern T, Dandekar T. Toward a systemic understanding of Listeria monocytogenes metabolism during infection. *Front Microbiol* 2012; **3**: 23.

102 Lecours MP, Gottschalk M, Houde M, Lemire P, Fittipaldi N, Segura M. Critical role for Streptococcus suis cell wall modifications and suilysin in resistance to complement-dependent killing by dendritic cells. *J Infect Dis* 2011; **204**: 919–929.

103 Chabot-Roy G, Willson P, Segura M, Lacouture S, Gottschalk M. Phagocytosis and killing of Streptococcus suis by porcine neutrophils. *Microb Pathog* 2006; **41**: 21–32.

104 Stefaniuk M, Gualda EJ, Pawlowska M, Legutko D, Matryba P, Koza P *et al.* Light-sheet microscopy imaging of a whole cleared rat brain with Thy1-GFP transgene. *Sci Rep* 2016; **6**: 28209.

105 Pan C, Cai R, Quacquarelli FP, Ghasemigharagoz A, Lourbopoulos A, Matryba P *et al.* Shrinkage-mediated imaging of entire organs and organisms using uDISCO. *Nat Methods* 2016; **13**: 859–67.

106 Soderblom C, Lee D-H, Dawood A, Carballosa M, Jimena Santamaria A, Benavides FD *et al.* 3D Imaging of Axons in Transparent Spinal Cords from Rodents and Nonhuman Primates(,). *eNeuro* 2015; **2**. doi:10.1523/ENEURO.0001-15.2015.

107 Udan RS, Piazza VG, Hsu C-WC -w., Hadjantonakis a.-KA-K, Dickinson ME. Quantitative imaging of cell dynamics in mouse embryos using light-sheet microscopy. *Development* 2014; **141**: 4406–4414.

108 Glaser AK, Reder NP, Chen Y, McCarty EF, Yin C, Wei L *et al.* Light-sheet microscopy for slide-free non-destructive pathology of large clinical specimens. *Nat Biomed Eng* 2017; **1**: s41551-17.

109 Weninger WJ, Geyer SH, Mohun TJ, Rasskin-Gutman D, Matsui T, Ribeiro I *et al.* High-resolution episcopic microscopy: a rapid technique for high detailed 3D analysis of gene activity in the context of tissue architecture and morphology. *Anat Embryol (Berl)* 2006; **211**: 213–221.

110 Ewald AJ, Mcbride H, Reddington M, Fraser SE, Kerschmann R. Surface imaging microscopy, an automated method for visualizing whole embryo samples in three dimensions at high resolution. *Dev Dyn* 2002; **225**: 369–375.

111 Barondes SH, Barondes S., Barondes S., Chirgwin J., Kornfeld S, Mole J. *et al.* Bifunctional properties of lectins: lectins redefined. *Trends Biochem Sci* 1988; **13**: 480–2.

112 Jährling N, Becker K, Dodt H-U. 3D-reconstruction of blood vessels by ultramicroscopy. *Organogenesis* 2009; **5**: 227–30.

113 Robertson RT, Levine ST, Haynes SM, Gutierrez P, Baratta JL, Tan Z *et al.* Use of labeled tomato lectin for imaging vasculature structures. *Histochem Cell Biol* 2014; **143**: 225–234.

114 Wiley JA, Richert LE, Swain SD, Harmsen AA, Barnard DL, Randall TD *et al.* Inducible bronchus-associated lymphoid tissue elicited by a protein cage nanoparticle enhances protection in mice against diverse respiratory viruses. *PLoS One* 2009; **4**: e7142.

Affidavit

I herewith declare that I autonomously carried out the PhD thesis entitled: Induction of bronchus-associated lymphoid tissue (BALT) by common zoonotic microorganisms, and establishment of a method for its quantification in whole lung lobes.

All bacteria that were used for BALT induction experiments were prepared in collaboration with Prof. Dr. Peter Valentin-Weigand's laboratory at the Institute for Microbiology, University of Veterinary Medicine Hannover, Hannover, Germany. Translation of the project summary to German (Zusammenfassung) was kindly done by Dr. Henrike Fleige, of the Institute of Immunology, Hannover Medical School.

I did not receive any assistance in return for payment by consulting agencies or any other person. No one received any kind of payment for direct or indirect assistance in correlation to the content of the submitted thesis.

I conducted the project at the Institute of Immunology, Hannover Medical School, Hannover, Germany.

The thesis has not been submitted elsewhere for an exam, as thesis or for evaluation in a similar context.

I hereby affirm the above statements to be complete and true to the best of my knowledge.

Date, signature

Acknowledgements

I would like to thank Prof. Dr. Reinhold Förster for the opportunity to work in his lab, his great supervision, and for reviewing my thesis. In addition, I would like to thank Prof. Dr. Peter Valentin-Weigand and Prof. Dr. Susanne Häußler for their supervision and reviewing my thesis; Prof. Jens Stein for reviewing my thesis; and all members of the PhD commission.

I would like to acknowledge the financial support from the Lichtenberg-Stipend (through TiHo), and Institute of Immunology, MHH.

I would like to thank the Hannover Graduate School for Veterinary, Pathobiology, Neuroinfectiology, and Translational Medicine (HGNI) administrative office (Prof. Dr. Beatrice Grummer, Dr. Tina Selle, and Tanja Czeslik, as well as former members) for their help in guiding and reminding me, always in time, the requirements for this study. And also the Akademisches Auslandsamt team (Dr. Christine Winter, Maritta Ledwoch and Johanna Knoll) for their moral support, and of amazing excursions!

I would like to thank Dr. Sabine Johann, Simone Zimmer and Sabine Tönnies (Center for infection Biology – ZIB office and Institute of Immunology secretariat office, MHH) for their help and moral support to me and my family throughout my studies.

I would like to thank Dr. Henrike Fleige for in training me with various experiment procedures. She was always available to help and advice. Similarly, I would like to thank all members (present and those who left) of AG Förster for their constructive comments during weekly meetings whenever I presented results. The same goes to all members (present and those who left) of the Institute of Immunology, MHH. Every one of you provided me with a lot of support in different ways.

I would like to also thank Prof. Dr. Ulrich Kalinke and his lab (TWINCORE, Hannover) for kindly providing adaptor molecule knock out mice; and Prof. Dr. Gerd Sutter (LMU, Munich) for kindly providing MVA virus used in my experiments. And also, Prof. Dr. Peter Valenin-Weigand and Kristin Laarmann (Institute of Microbiology, TiHo) for their help with preparation of bacteria strains used in my experiments.

A special thanks to my wife, Noella, for her moral support (a lot of it). Together with Josiah and Timothy, we consider ourselves blessed to have you around! In addition, I would like to thank my parents and siblings in Malawi, for your encouragement and allowing me to travel and stay away from you all for a while.

Above all I would like to thank God for the gift of life and many opportunities past, present and future.